01 Jul 2021

Numerical Investigation of the Thermo-Hydraulic Performance of Water-Based Nanofluids in a Dimpled Channel Flow using Al_2O_3, CuO, and Hybrid Al_2O_3-CuO as Nanoparticles

Farid Ahmed

Md Atrehar Abir

Muhtasim Fuad

Farhana Akter

et. al. For a complete list of authors, see https://scholarsmine.mst.edu/nuclear_facwork/496

Recommended Citation

F. Ahmed et al., "Numerical Investigation of the Thermo-Hydraulic Performance of Water-Based Nanofluids in a Dimpled Channel Flow using Al_2O_3, CuO, and Hybrid Al_2O_3-CuO as Nanoparticles," *Heat Transfer*, vol. 50, no. 5, pp. 5080-5105, Wiley Open Access, Jul 2021.
The definitive version is available at https://doi.org/10.1002/htj.22116

Received: 20 October 2020 | Revised: 15 February 2021 | Accepted: 19 February 2021

DOI: 10.1002/htj.22116

RESEARCH ARTICLE

HEAT TRANSFER WILEY

Numerical investigation of the thermo-hydraulic performance of water-based nanofluids in a dimpled channel flow using Al_2O_3, CuO, and hybrid Al_2O_3–CuO as nanoparticles

Farid Ahmed[1] | **Md Atrehar Abir**[2] | **Muhtasim Fuad**[1] | **Farhana Akter**[3] | **Palash K. Bhowmik**[4] | **Syed Bahauddin Alam**[4] | **Dinesh Kumar**[5]

[1]Department of Nuclear Science and Engineering, Military Institute of Science and Technology, Dhaka, Bangladesh

[2]Department of Mechanical and Production Engineering, Islamic University of Technology, Gazipur, Bangladesh

[3]Department of Physics, National University, Gazipur, Bangladesh

[4]Nuclear Engineering and Radiation Science, Missouri University of Science and Technology, Rolla, United States, USA

[5]Materials Research and Technology, Luxembourg Institute of Science and Technology, Esch-sur-Alzette, LU, Luxembourg

Correspondence
Farid Ahmed, Military Institute of Science and Technology, Dhaka, Bangladesh.
Email: faridrakib3@gmail.com

Abstract

In this study, the authors study the impact of spherical dimple surfaces and nanofluid coolants on heat transfer and pressure drop. The main objective of this paper is to evaluate the thermal performance of nanofluids with respect to different Reynolds numbers (*Re*) and nanoparticle compositions in dimpled channel flow. Water-based nanofluids with Al_2O_3, CuO, and Al_2O_3–CuO nanoparticles are considered for this investigation with 1%, 2%, and 4% volume fraction for each nanofluid. The simulations are conducted at low Reynolds numbers varying from 500 to 1250, assuming constant and uniform heat flux. The effective properties of nanofluids are estimated using models proposed in the literature and are combined with the computational fluid dynamics solver ANSYS Fluent for the analysis. The results are discussed in terms of heat transfer coefficient, temperature distributions, pressure drop, Nusselt number, friction factors, and performance criterion for all the cases. For all cases of different nanoparticle compositions, the heat transfer

coefficient was seen as 35%–46% higher for the dimpled channel in comparison with the smooth channel. Besides, it was observed that with increasing volume fraction, the values of heat transfer and pressure drop were increased. With a maximum of 25.18% increase in the thermal performance, the 1% Al_2O_3/water was found to be the best performing nanofluid at $Re = 500$ in the dimpled channel flow.

KEYWORDS
CFD, dimple surface, heat exchanger, heat transfer, hybrid nanofluid

1 | INTRODUCTION

The advent of the 21st century demands compact and smaller tools. More micro-equipments, including micropumps, microsensors, micro-turbines, and so forth, have been produced by industry.[1] The efficiency of such engineering components highly depends on the cooling performance inhibiting and prolonging their durability.[2,3] Therefore, the maximum working temperature and even distribution of heat is an important concern for almost all industrial applications. Therefore, research has been shifted to produce greater thermal efficiencies at the micro level.[4] The long life and dependability of these tools are influenced by several factors. The technology industries need components with compact devices.[5,6] Hwang et al.[7] talk about the increasing use of micro-turbines in industrial applications, which have a smaller efficiency in particular. Due to the reduced length of the flow channels, these systems operate at the Reynolds number of the lowest scale. He urged a more detailed analysis of this flow along with its thermal transmission characteristics under low Reynolds number. In his research, he implemented a stamping process in the flow channels with the required range of Reynolds numbers to produce dimples and protrusions.[7–10] This technology of channel with the reduced flow is useful to extract heat from these micro-devices[11] because of its high volume surface and large convective coefficient.[12] These channels can operate as high heat dissipators and rising surface thermal gradients and have a different mechanism than traditional channels. Here, the stress is applied to an internal coolant to allow the flow to circulate along the lining of the tank, which enhances the transfer performance. The large area allows the dissipation of vast amounts of heat. There were some shortcomings when evaluating such a channel with a reduced length. A careful evaluation of the application of the Navier–Strokes equation and the continuum equation is required as the distance from the particle is extremely small. In general, the use of gas contains considerable errors, but for liquid, measurements are accurate to the degree that is confirmed by several authors[12,13] at the Reynolds number of approximately 2300.

In the last few decades, researchers have introduced a range of methods for heat enhancement analysis. As mentioned earlier, the shapes of the fins can be varied across various parameters to support the heat transfer coefficient (HTC). Different geometries can be used to adjust the surface of the channel to boost performance.[14] A dimpled surface exhibits relatively higher fluid mixing and so a higher pressure loss on the wall surface.[15] The first experiment

using dimple surfaces was conducted on blades for gas turbine cooling.[16] There are two different kinds of dimple shapes (spherical and tear-drop shapes) discussed in the literature. A comparison between smooth and dimpled surface analysis is shown in Chyu et al.'s[17] paper. The results show that a surface with dimples has 2.5 times higher heat transmission. These enhanced surfaces improve the coefficient of heat flow and increase the level of friction. A boundary layer over the surface is formed that contributes to distortion and hence reduces the region of heat transfer. Li et al.[18] investigated the pressure loss and heat transfer properties for helically dimpled surfaces, and it was confirmed by Siddique et al.[19] This design interrupted the original flow pattern, which enhanced streamlined turbulence. Therefore, in comparison with the flat tubing, the HTCs reported were 1.74 and 2.48 times higher. Thermal efficiency can be drastically improved by adding nanofluid media. Nanofluids have exceptional thermophysical properties, including high thermal conductivity in heat transfer applications. Nanofluids refer to nanoparticles colloids suspended with increased flexibility in a base stream.[21–25] A huge amount of focus has been paid to the hybrid convective heat transfer. A good number of studies have been conducted to study the thermal behavior of nanofluids and hybrid nanofluids.[26–28] Xuan and Li[29] showed that CuO-H_2O nanofluid's heat transfer performance had been improved than that of the base fluid. Moshizi et al.[30] tested the thermal properties of Al_2O_3–water nanofluid by utilizing continuous thermal flow in a pipeline. Owing to slip velocity on tube walls, they found increased heat transfer efficiency and pressure gradient efficiency. Akbari et al.[3] conducted their study on the thermal transfer of CuO nanofluid in a two-phase microtube. Furthermore, several studies have been conducted on the hybrid nanofluids both numerically[2,31–41] and experimentally.[42–46]

To propose and design a better performing heat exchanger, it is indeed worthwhile to understand how thermal performances of the heat exchanger can be numerically impacted by alternative coolants and surfaces.[47] Therefore, in this paper, a compound technique of heat transfer enhancement is shown, which involves both the modification of geometry and improvement in the coolant. The paper evaluates the thermal performance of both nanofluids (CuO + water, Al_2O_3 + water) and hybrid nanofluids (Al_2O_3−CuO + water)[48] as well as the impacts of spherical dimpled surfaces in the channel with reduced computational length using computational methods. The variation of entropy generation for different coolants was discussed to give detailed information about the coolant's performance. With the impact of volume fractions and *Re* in each nanofluid, we observe the suitable volume fraction to reach maximum thermal performance in the channel flow.

2 | THERMOPHYSICAL PROPERTIES OF THE NANOFLUIDS

In recent years, significant works of literature are published proposing models to estimate the effective thermo-physical property of nanofluids.[49–52] The fact that nanofluid thermo-physical behaviors have been systematically investigated and that controversial experimental information lacks precision. A single-phase method for the calculation of thermo-physical properties is selected due to the large acceptance in the literature.[53–55] The presumption of thermal balance for the particles is established, together with assuming that the fluid and the particles are not velocity different.[54,56–59] That assumption shows that the correlation of convective heat transfer for single-phase flow can also be used if only the effective nanofluid characteristics merge with the thermal-physical property calculated at reference temperatures.[60,61]

For practical applications of oxide particles of nanofluids higher than 40 nm, the model proposed by Maïga et al.,[62] is considered a better priority. In this model, the effective properties of a nanofluid[63] can be estimated from the following set of equations[23]:

$$\rho_{\mathrm{hnf}} = (1-\varphi)\rho_{\mathrm{bf}} + \varphi\rho_{\mathrm{p}}, \tag{1}$$

$$(\rho Cp)_{\mathrm{hnf}} = (1-\varphi)(\rho C_{\mathrm{p}})_{\mathrm{f}} + \varphi(\rho C_{\mathrm{p}})_{np}, \tag{2}$$

$$(\rho\beta)_{\mathrm{hnf}} = (1-\varphi)(\rho\beta)_{\mathrm{f}} + \varphi(\rho C_{\mathrm{p}})_{np}, \tag{3}$$

$$\alpha_{\mathrm{hnf}} = \frac{k_{\mathrm{hnf}}}{(\rho Cp)_{\mathrm{hnf}}}, \tag{4}$$

$$k_{\mathrm{hnf}} = \frac{k_{\mathrm{np}} + (m-1)k_{\mathrm{f}} - (m-1)(k_{\mathrm{f}} - k_{\mathrm{np}})\varphi}{k_{\mathrm{np}} + (m-1)k_{\mathrm{f}} + (k_{\mathrm{f}} - k_{\mathrm{np}})\varphi}k_{\mathrm{f}}, \tag{5}$$

$$\mu_{\mathrm{hnf}} = \frac{\mu_{\mathrm{f}}}{(1-\phi)^{2.5}}, \tag{6}$$

$$\varphi = \varphi Al_2O_3 + \varphi CuO, \tag{7}$$

$$\rho_{\mathrm{np}} = \frac{\varphi Al_2O_3\rho Al_2O_3 + \varphi CuO(C_{\mathrm{p}})CuO}{\varphi}, \tag{8}$$

$$\left(C_{\mathrm{p}}\right)_{\mathrm{np}} = \frac{\varphi Al_2O_3(C_{\mathrm{p}})Al_2O_3 + \varphi CuO(C_{\mathrm{p}})CuO}{\varphi}, \tag{9}$$

$$\beta_{\mathrm{np}} = \frac{\varphi Al_2O_3\beta Al_2O_3 + \varphi CuO\beta CuO}{\varphi}, \tag{10}$$

$$k_{\mathrm{np}} = \frac{\varphi Al_2O_3\beta Al_2O_3 + \varphi CuOkCuO}{\varphi}. \tag{11}$$

Due to the restriction of experimental information, the effective density of fluids was estimated using classical two-phase flow formulations. The density remains constant with the temperature.[54,56–58,62,64] For estimating the specific heat of nanofluids some expressions are recommended in References [54,56–58,62,64,65]. Due to having a lack of appropriate experimental data for nanofluids, the viscosity was evaluated using the Brinkman model,[66] and the thermal conductivity was evaluated using Hamilton and Crosser, and Yu and choi[67,68] correlation. The model is assumed to be precise with a maximum deviation of 1.04% up to 14% volume fraction. For evaluating the properties of hybrid nanofluid, Equations (1)–(11) were used, which is essentially a modified form of the nanofluid's thermophysical properties.[69,70] The mixture ratio was maintained Al_2O_3/water to CuO/water ($\phi Al_2O_3/\phi CuO$) to be 50%/50%.

TABLE 1 Effective properties of aluminum oxide (Al_2O_3) and copper oxide (CuO)[72-75]

Type of material	Density (ρ) (kg/m^3)	Specific heat (C_p) (J/kg K)	Thermal conductivity (k) (W/m K)
Al_2O_3 (45 nm)	3600	765	36
CuO (29 nm)	6500	533	17.65

TABLE 2 Effective properties of Al_2O_3/water

	Al_2O_3/water		
	$\phi = 1\%$	$\phi = 2\%$	$\phi = 4\%$
ρ (kg/m^3)	1023.129	1049.15	1101.216
C_p (J/kg K)	4058.87	3944.7	3732.56
k (W/m K)	0.63	0.648	0.685
μ (Pa.s)	9.14×10^{-4}	9.37×10^{-4}	9.87×10^{-4}

TABLE 3 Effective properties of CuO/water

	CuO/water		
	$\phi = 1\%$	$\phi = 2\%$	$\phi = 4\%$
ρ (kg/m^3)	1052.129	1107.158	1217.216
C_p (J/kg K)	3953.75	3750.89	3400.2
k (W/m K)	0.629	0.646	0.681
μ (Pa.s)	9.14×10^{-4}	9.37×10^{-4}	9.87×10^{-4}

TABLE 4 Effective properties of Al_2O_3–CuO/water

	Al_2O_3–CuO/water		
	$\phi = 1\%$	$\phi = 2\%$	$\phi = 4\%$
ρ (kg/m^3)	1037.62	1078.15	1159.21
C_p (J/kg K)	4006.88	3847.66	3559.35
k (W/m K)	0.63	0.648	0.684
μ (Pa.s)	9.14×10^{-4}	9.37×10^{-4}	9.87×10^{-4}

Table 1 represents the properties of nanoparticles at 298K. Tables 2–4[71] represent the thermophysical properties at 298K for three different nanofluids considered in this study.

3 | MATHEMATICAL MODELING

The computational fluid dynamics (CFD) simulations are carried out using ANSYS Fluent for the dimpled geometry with continuity, momentum equation, and energy conservation.[43]

The fluid is assumed as Newtonian and incompressible when considering the mathematical implications. The steady-state Navier–Stokes equations are solved for the dimpled channel and smooth channel shape for fluid flow and thermal transfer analysis. The nanoparticles are considered to be spherical shaped and uniformly mixed.

The governing equations are as follows[76]:

$$\nabla . (\rho . \vec{v}) = 0, \tag{12}$$

$$\nabla.(\rho.\vec{v}.\vec{v}) = -\nabla p + \nabla.\left(\mu\left[(\nabla\vec{v} + \nabla\vec{v}^{T}) - \frac{2}{3}\nabla.\vec{v}I\right]\right) + \rho\vec{g}, \tag{13}$$

$$\nabla.(\vec{v}(\rho E + p)) = \nabla.\left(k_{eff}\nabla T - h\vec{J} + \left(\mu\left[(\nabla\vec{v} + \nabla\vec{v}^{T}) - \frac{2}{3}\nabla.\vec{v}I\right].\vec{v}\right)\right). \tag{14}$$

3.1 | Configuration of geometry

The flow domain is considered to be conventional channels with 110 mm as a channel length. The diameter range for different subchannels are illustrated in Table 5.

The dimpled surface diameter is kept constant and is equal to 5 mm. The dimples along the streamwise directions (x/d) are kept at 2.00, whereas the dimples along the spanwise direction (y/d) are kept to be 5.25. The computational geometry is illustrated in Figure 1.

TABLE 5 Representation of classification scheme according to the diameter[77]

Name of channel	Range of hydraulic diameter
Conventionnel channels	$D_h > 3\,mm$
Minichannels	$3\,mm \geq D_h > 200\,\mu m$
Microchannels	$200\,\mu m \geq D_h > 10\,\mu m$
Transitional channels	$10\,\mu m \geq D_h > 0.10\,\mu m$

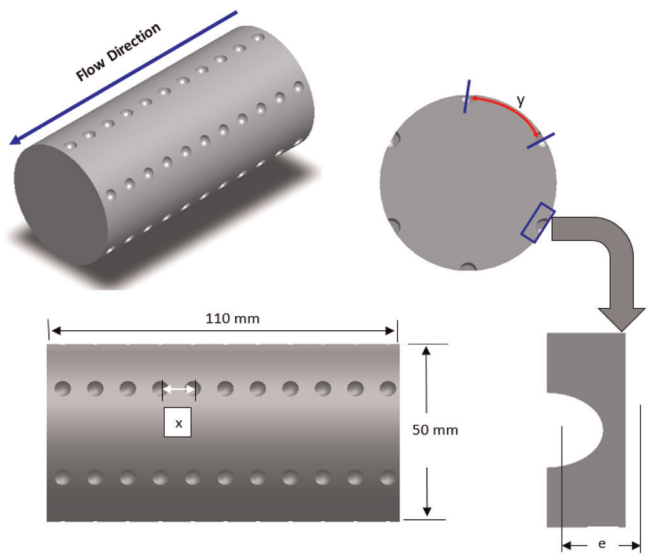

FIGURE 1 Computational domain [Color figure can be viewed at wileyonlinelibrary.com]

3.2 | Mesh generation and refinement analysis

For better accuracy in the CFD simulations, polyhedral meshes were generated. Dense grids were generated near the wall and the dimpled surfaces to capture the thermal boundary, velocity gradient as well as to predict boundary layer separation accurately. The skewness factor and orthogonal quality were maintained to be below 0.18 and 0.88, respectively. Figure 2 shows the polyhedral grid generation over the dimpled geometry. For the smooth geometry, hexahedral meshes were implemented on the smooth channel with near-wall treatment along the boundaries. Dense grids were implemented to capture the boundary layer separations and thermal boundary layers precisely. The aspect ratio of the hexahedral mesh was kept at 4.00 with orthogonal quality 0.95. Figure 3 shows the hexahedral mesh over the smooth channel. Improvement of mesh models is regulated with the refining of the grids since ANSYS Fluent uses the Finite Volume Method to perform computation. To evaluate the performance of grids, mesh independence tests were performed where five different types of grids were assessed, varying the element sizes. The mesh refinement ratio (MRR) was defined as the improvement of grids in between two consecutive meshes (like G2/G1). Table 6 shows the performance of different grids to produce better accuracy. It is evident from the table that Grid 5 (G5) produces the highest accuracy with 0.08% and 0.13% errors in the dimpled channel and smooth channel consecutively. Besides, it is evident from Figure 4 that the variation of element size is not leading to any noticeable differences in the outlet radial velocity profile of the dimpled channel. Hence, from the above discussion, the G5 mesh model is used in this study for the simulations and results.

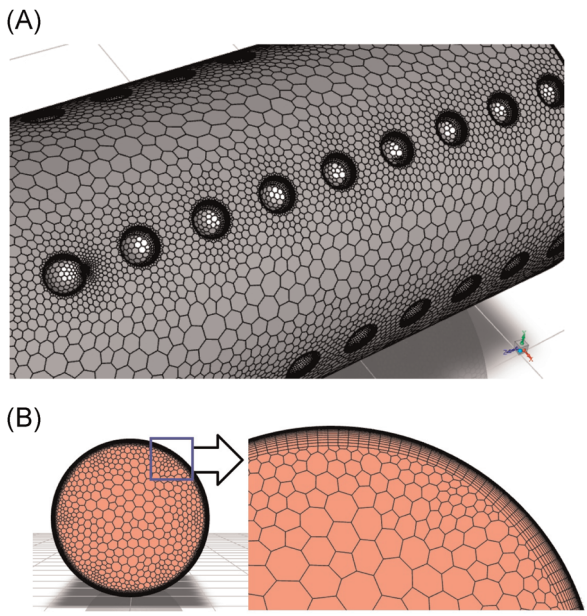

FIGURE 2 Computational domain and mesh for the smooth channel: surface (A) and cross-section (B) [Color figure can be viewed at wileyonlinelibrary.com]

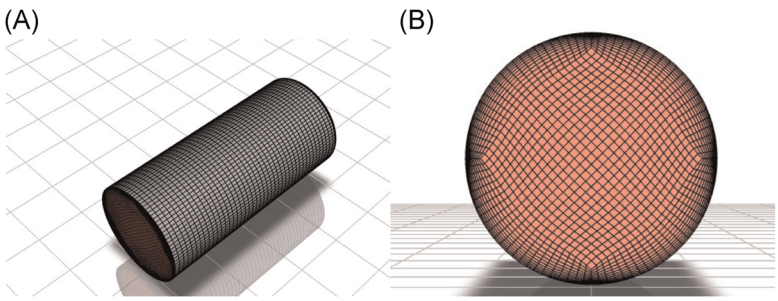

FIGURE 3 Computational domain and mesh for the dimpled channel: surface (A) and cross-section (B) [Color figure can be viewed at wileyonlinelibrary.com]

TABLE 6 Impact of grid refinement on dimpled and smooth channel

Step	MRR	% Error for the dimpled channel (ΔNu_{avg})	% Error for the smooth channel (ΔNu_{avg})
Grid (2 to 1)	1.033	2.96	3.23
Grid (3 to 2)	1.059	2.59	2.67
Grid (4 to 3)	13.07	0.33	0.76
Grid (5 to 4)	1.85	0.08	0.13

Abbreviation: MRR, mesh refinement ratio.

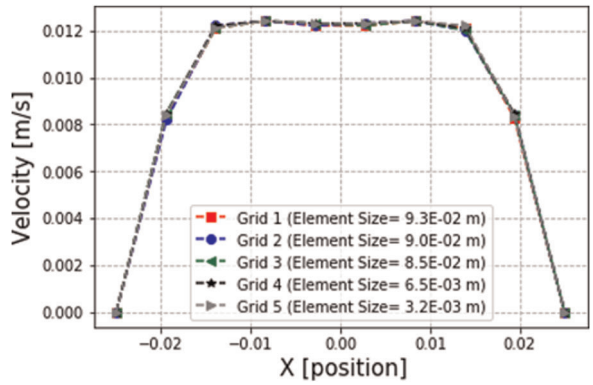

FIGURE 4 Variation of velocity profile with different element size at $Re = 500$ for dimpled channel [Color figure can be viewed at wileyonlinelibrary.com]

3.3 | Modeling and simulation details

The computational analysis was performed under a constant and uniform heat flux (=10 kW/m^2). By varying Reynolds numbers between 500 and 1250, the inlet velocity profiles were varied within the channel. The inlet temperature for the coolants is assumed to be 298K, whereas the gauge outlet pressure is kept to be zero. An implicit solver is considered in solving the governing equations. The root mean square (RMS) values for momentum and continuity equations are targeted up to 10^{-6} and 10^{-8} for the energy equation in ANSYS Fluent. Basic formulations for the

analysis: average HTC, average Nusselt number, pressure drop, and performance evaluation criteria (PEC) have been utilized for the calculations.[73,78–80]

4 | VALIDATION OF THE CFD MODEL

The smooth channel was first used for simulation using the exact dimensions of the dimpled model for validating the dimple model.[6] The results of the smooth channel were compared from the results of Stephan's and PreuBer's existing Nu correlations for circular pipes.[81,82] The correlation used for the Nusselt number calculation and for the comparison is illustrated in the following equation:

$$Nu = 4.364 + \frac{0.\ 086(Re\,Pr\,D_h/L)^{1.33}}{1 + 0.1 \quad Pr(Re\,D_h/L)^{0.83}}, \tag{15}$$

$$\text{where } 0 < Re < 2300.$$

In Figure 5, the results from our simulations are compared with the reference solution.[81] It is evident from the figure that present study aligns precisely with the Stephan correlation. A maximum error of 3.5% in the average Nusselt (Nu_{avg}) at $Re = 1250$ was found. The assumption could be made from the simulation results that the accurate predictions of the rest of the simulation for the proposed dimple model are possible, which confirm the validity of the dimpled model in terms of accuracy and precision. The computed values of T_m are also compared with the results from the Energy Balance Equation (16) for the dimpled channel flow.[83] To evaluate and compare the local mean temperature of the fluid, the value of the Re was selected to be 750 and 1250. The comparison in results is illustrated in Figure 6, which shows an acceptable agreement with Equation (16) with a maximum deviation of 1.02% at $Z =$ 0.03 m for $Re = 750$ and 1.65% at $Z = 0.05$ m $Re = 1250$.

From the energy balance equation,[83] the mean temperature (T_m) profile (used for comparison of results) can be expressed as

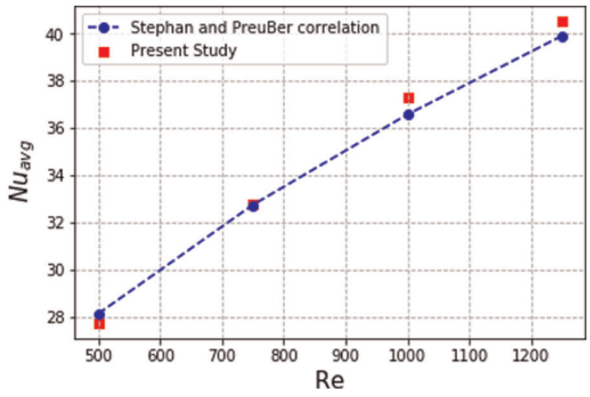

FIGURE 5 Validation of the results with Stephan correlation[81] [Color figure can be viewed at wileyonlinelibrary.com]

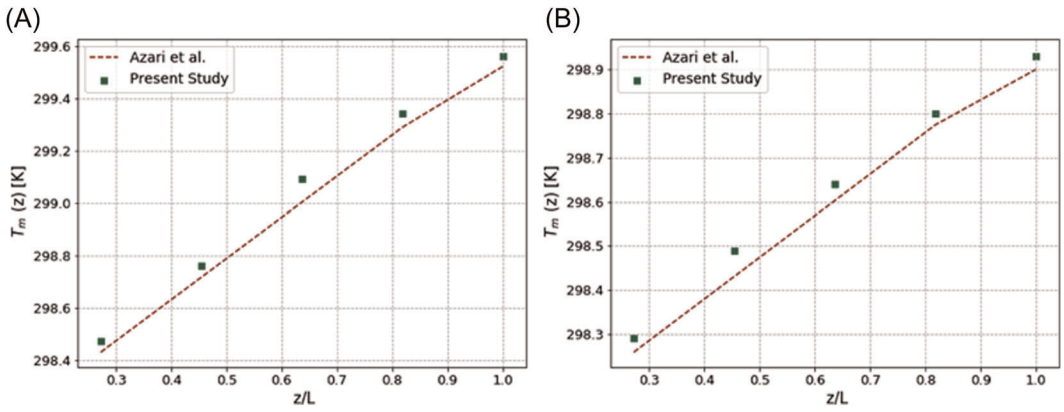

FIGURE 6 Difference of the mean temperature between present study and the study of[71,83] (A) $Re = 750$ and (B) $Re = 1250$ [Color figure can be viewed at wileyonlinelibrary.com]

$$T_{\mathrm{m}}(z) = T_{\mathrm{m}}(\dot{m}) + \frac{\ddot{q}\pi D_{\mathrm{h}}}{\dot{m}c_p} z. \tag{16}$$

Moreover, the measured local Nusselt number was compared with the shah correlation for the implantation in the case of dimpled flow.[84] Equations (17) and (18) indicate the Shah equation that refers to the smooth circular channel of the laminar flow. Since there were no correlations accessible to laminar flow for dimple cases, the findings were compared with the Shah correlation.[84] After evaluating Figure 7, it is clear that dimpled cases are strongly linked to the conventional correlation with a maximum deviation of 7.2%. The maximum variation was noticed at $Z = 0.03$ m (in the axial direction) at $Re = 250$.

Using the Shah correlation,[84] the Nusselt number can be formulated as

$$Nu = 1.953\left(Re\,Pr\frac{d}{x}\right)^{\frac{1}{3}}, \tag{17}$$

$$\text{for } \left(Re\,Pr\frac{d}{x}\right) \geq 33.33.$$

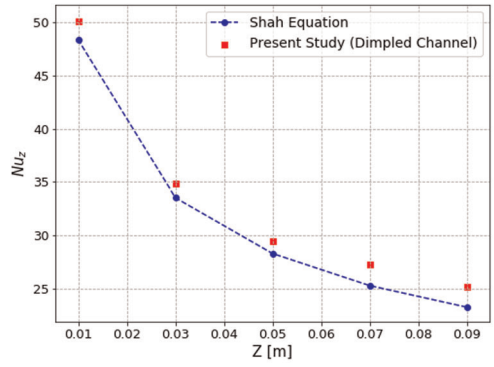

FIGURE 7 Results comparison: Dimpled surface case and a traditional correlation (Shah correlation) for base fluid at $Re = 500$ [Color figure can be viewed at wileyonlinelibrary.com]

$$Nu = 4.364 + 0.0722\left(Re\,Pr\frac{d}{x}\right), \quad \text{for } \left(Re\,Pr\frac{d}{x}\right) < 33.33. \tag{18}$$

Upon investigating both local and global thermo-physical parameters and assessing the accuracy, it is evident that the present CFD model could implore the validity of the study. Therefore, the remaining simulations were investigated following the proposed computational domain.

5 | RESULT AND DISCUSSION

In this section, first, we evaluate the heat transfer performance in the dimpled channel with a spherical shape (described earlier) for base fluid as water. Further, a comprehensive study will be provided among Al_2O_3/water, Al_2O_3–CuO/water ($\phi Al_2O_3/\phi CuO = 1/1$), and CuO/water to justify the thermal performance of hybrid nanofluid and to compare the thermal performance of each nanofluid. The value of *Re* is varied from 500 to 1250 during the investigation.

5.1 | Analysis of flow characteristics at different *Re* and volume fraction

Analyzing Figure 8, it is observed that the maximum velocity has occurred in the central region of the velocity profile. However, the velocity gradually decreases from the center to the tube wall and the minimum velocity is identified at the leeward surface of dimples. Moreover, the velocity tends to increase with the windward surfaces of the dimple and decrease with the leeward surface. This phenomenon is likely to occur due to the shrinkage of the flow channel at the windward surface of dimples, which results in the increase of velocity. Contrary to the windward surface, at the leeward surface of the dimples, the flow channel gets expanded which

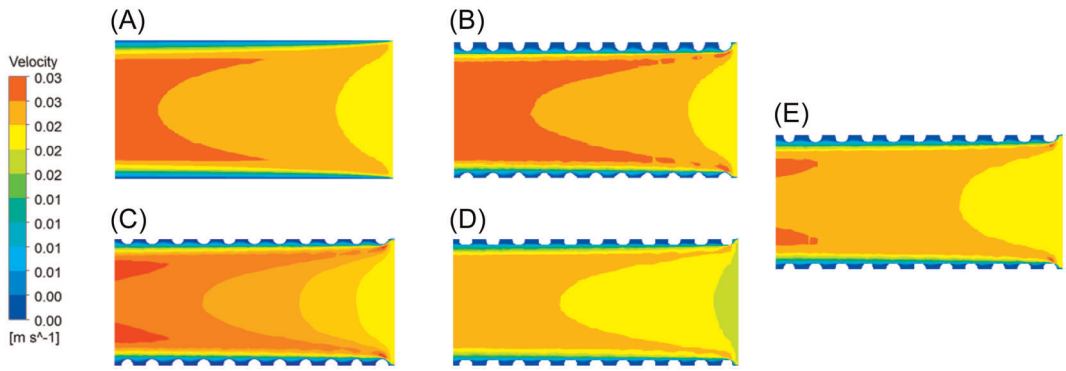

FIGURE 8 Velocity distribution for different nanofluids along the center region at $Re = 1250$. (A) Smooth channel, (B) dimple channel, (C) dimple channel + 4% alumina vol fraction, (D) dimple channel + 4% CuO vol fraction, and (E) dimple channel + 4% Al_2CO_3–CuO vol fraction [Color figure can be viewed at wileyonlinelibrary.com]

causes the velocity to decrease. Because of having such variation periodically, improvement is observed in the momentum exchange, and enhancement of fluid flow mixing occurs between mainstream zone and near-wall zone. The magnitude of velocity is found maximum at the central region of the domain, whereas the minimum value is identified in between the spaces of two consecutive dimples. Due to the presence of dimples, both the blocking effect and impingement effect are perceived, which resulted in the interruption of the boundary layer.

Besides, it is evident from Figure 8 that the smooth channel reached a fully developed laminar flow structure earlier, followed by the dimpled channel, and further followed by the dimpled channel with 4% Al_2O_3/water nanofluid. It is recognized that dimpled channel with Al_2O_3–CuO hybrid nanofluid delayed the most to reach fully laminar developed flow followed by dimpled channel with CuO/water nanofluid. Figure 9 displays the radial distribution of velocity at the outlet region of computational domains at $Re = 1250$. Figure 9 concludes that velocity profile is not impacted by dispersion of nanoparticles to a base fluid for a negligible range of nanoparticle volume fraction (i.e., 1%–5%).[85,86]

5.2 | Heat transfer characteristics

5.2.1 | Temperature distribution

The HTC will be higher due to a decrease in wall temperature and an increase in bulk temperature of the fluid as the rest of the parameters are constant.[73,78–80] Hence the coolants with a lowered value of $(T_w - T_b)$ will acquire higher HTC. Figure 10 represents the magnitude of $(T_w - T_b)$ for different nanofluids at $Re = 500$, 750, 1000, and 1250.

From Figure 10A, it is evident that the magnitude of $(T_w - T_b)$ is highest for the smooth channel and gradually decreases for the dimpled channel. The lowest value is observed for 4% volume fraction, followed by 2%, 1%, and base fluid in the dimpled channel. Hence it can be concluded that a dimpled channel with a 4% volume fraction is capable of extracting more heat followed by 2%, 1%, and 0% in comparison with a smooth channel. A similar conclusion could

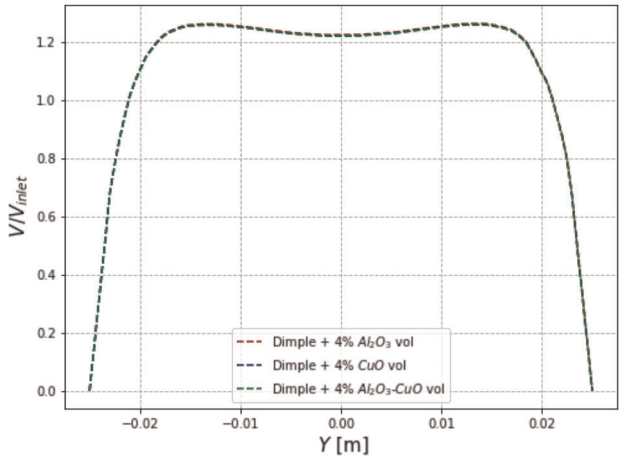

FIGURE 9 Radial distribution of velocity at an outlet for different nanofluids at $Re = 1250$ [Color figure can be viewed at wileyonlinelibrary.com]

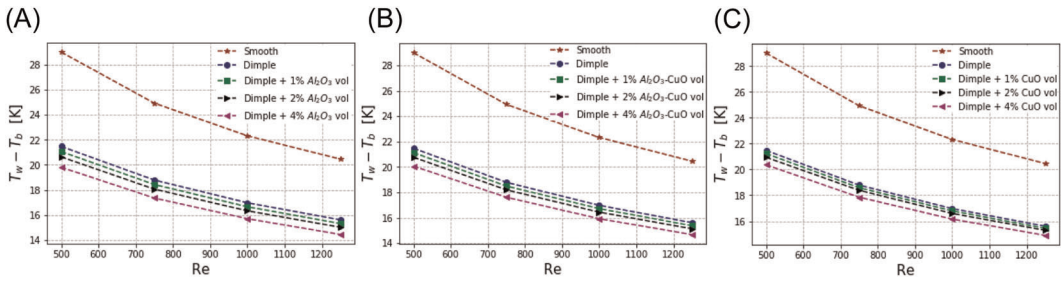

FIGURE 10 The magnitude of ($T_w - T_b$) for (A) Al_2O_3/water, (B) Al_2O_3–CuO/water, and (C) CuO/water [Color figure can be viewed at wileyonlinelibrary.com]

be drawn from Figure 10B that dimple with 4% Al_2O_3–CuO hybrid nanofluid is capable of extracting the highest heat followed by 2%, 1%, and 0%, whereas the lowest is observed for the smooth channel. From Figure 10C, a similar conclusion can be drawn that dimpled channel with 4% CuO extracts the highest heat followed by 2%, 1%, and base 0%, and the lowest value is identified for the smooth channel. Hence from the above discussion, the evaluation could be drawn that by increasing the volume fraction of nanoparticles, the capability of extracting heat increases.

Figure 11 represents the variation of wall temperature for different volume fractions of Al_2O_3–CuO/water nanofluid at $Re = 1250$. The figure shows the gradual increment of temperature in the wall of dimpled geometry along the flow direction.

5.2.2 | Study of HTC

The study of enhancement in heat transfer could be explained in terms of the improvement in thermophysical properties. For analyzing the properties enhancement ratio, as shown in Table 7, the calculation was progressed using the following equations:

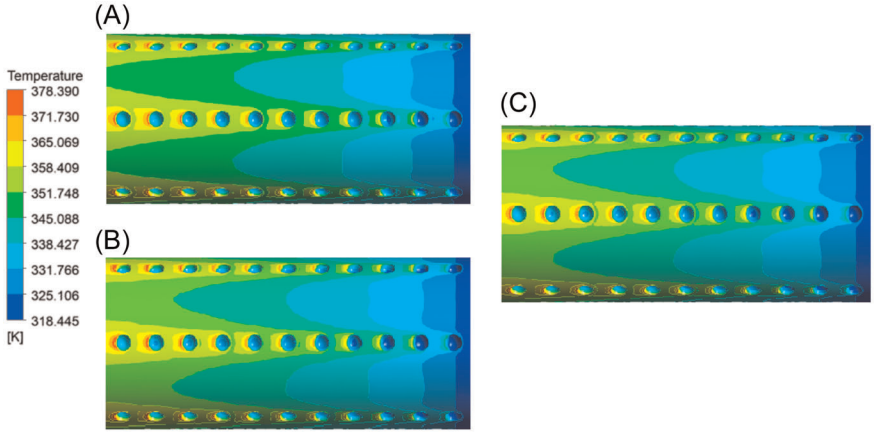

FIGURE 11 Temperature distribution at the wall of dimple channel for hybrid nanofluid at $Re = 1250$. (A) Al_2O_3–CuO 1% vol, (B) Al_2O_3–CuO 2% vol, and (C) Al_2O_3–CuO 4% vol [Color figure can be viewed at wileyonlinelibrary.com]

TABLE 7 Property enhancement ratio of different nanofluids investigated in the present study

Volume fraction	Al_2O_3/water	Al_2O_3–CuO/water	CuO/water
1% vol	1.003187	1.002773	1.001819
2% vol	1.006032	1.005039	1.003178
4% vol	1.010059	1.008159	1.004445

$$\text{Properties Enhancement Ratio (PER)} = \frac{\text{Thermal Conductivity Improvement Ratio}}{\text{Viscosity Improvement Ratio}}, \tag{19}$$

where

$$\text{Thermal Conductivity Improvement Ratio} = \frac{k_{\text{nf}}}{k_0}, \tag{20}$$

and

$$\text{Viscosity Improvement Ratio} = \frac{\mu_{nf}}{\mu_0}. \tag{21}$$

It is evident that a lower magnitude of $(T_w - T_b)$ will lead to a higher value of HTC.[73,78–80] Because of having surface roughness compared with the smooth channels, turbulence becomes predominant in the dimpled regime. The interruption of boundary layers created due to turbulence enables the dimpled channel to extract more heat. Hence the value of $(T_w - T_b)$ is found lower for dimpled cases. Assessing Figure 10, it is clear that 4% volume fractions of nanofluid are having a lower magnitude of $(T_w - T_b)$, and it gradually increases for 2%, 1%, and 0% in the dimpled channel. Therefore, the HTC should be highest for 4% volume fraction and lowest for the base fluid. The enhancement in HTC due to inclusions of nanoparticles could be explained with the property enhancement ratio (PER), as shown in Table 7. It is evident from the table that the value of PER gets increased with an increase in volume fraction, which results in the enhancement of HTC. Hence, a conclusion could be made from Figure 12 that with the increase of volume fraction as well as *Re*, the value of HTC increases. The maximum value is observed for the 4% volume fraction of each nanofluid at $Re = 1250$, and with the gradual decrement, the lowest HTC is identified for the base fluid with $Re = 500$.

The capability to extract more heat was evaluated with the help of the HTC for different coolants. The assessment could be drawn from Figure 13, which represents the value of HTC for different coolants as a function of *Re*. Figure 13A shows that the value of HTC is found highest for 1% vol of Al_2O_3/water followed by 1% Al_2O_3–CuO/water, followed by 1% CuO/water. Similar observations were found for both 2% and 4% vol of each coolant from Figure 13B,C. Among the nanofluids, the minimum HTC is observed for 1% vol CuO/water, and the maximum value of HTC is observed for 4% vol Al_2O_3/water. Therefore, a conclusion could be made that the ability to extract the heat is highest for Al_2O_3/water superseded by Al_2O_3–CuO/water and lowest for CuO/water. This is because the PER is found highest for Al_2O_3/water, followed by Al_2O_3–CuO/water and lowest for CuO/water, as illustrated in Table 7. Nevertheless, only the PER could not be enough to explain dramatic enhancement in heat transfer.

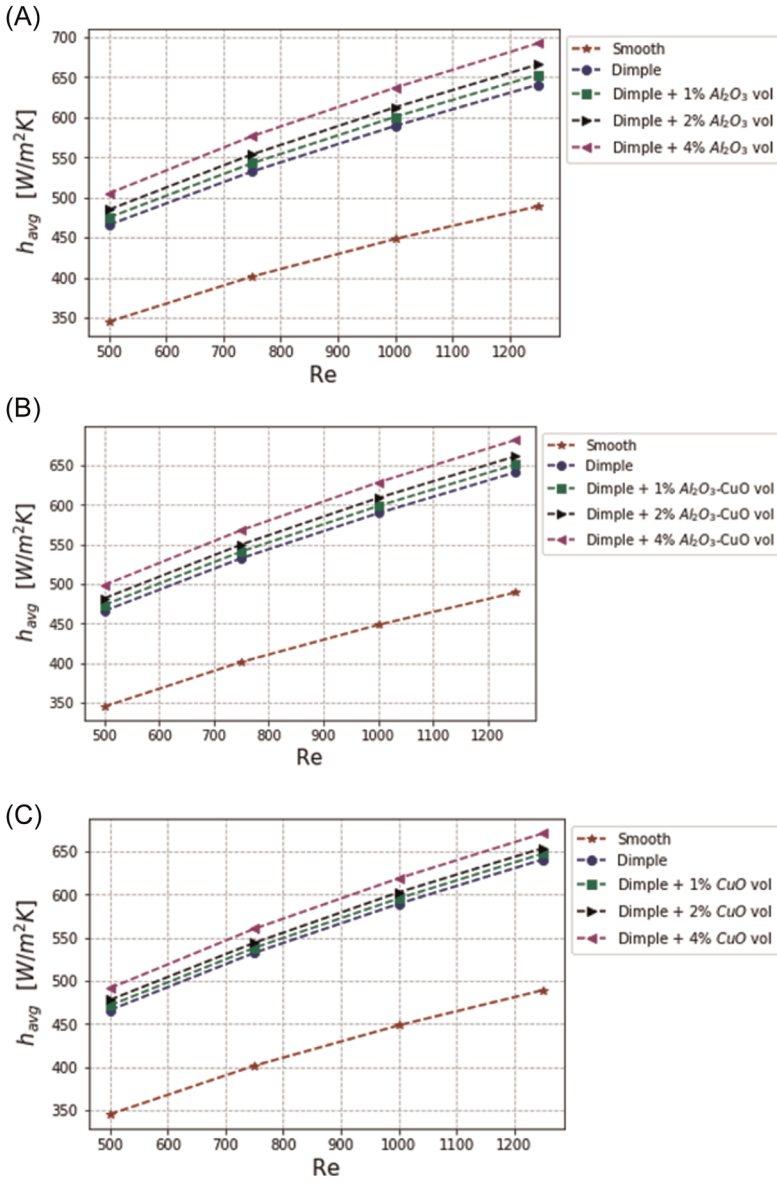

FIGURE 12 Heat transfer coefficients for different vol fractions of (A) Al_2O_3/water, (B) Al_2O_3–CuO/water, and (C) CuO/water [Color figure can be viewed at wileyonlinelibrary.com]

5.3 | Study of pressure drop

For ensuring better thermal efficiency, the evaluation of pressure drop is investigated in this study. Compared with the smooth channel, as shown in Figure 14, the dimpled channel is showing higher pressure drop due to the fluctuations in the velocity profile and turbulence created by the dimpled regions. Besides, it is identified from Figure 14A that 1% vol Al_2O_3/water is having the highest pressure drop, followed by 1% Al_2O_3–CuO/water, and the lowest is seen for 1% CuO/water. Similar observations could be found for 2% and 4% vol of each

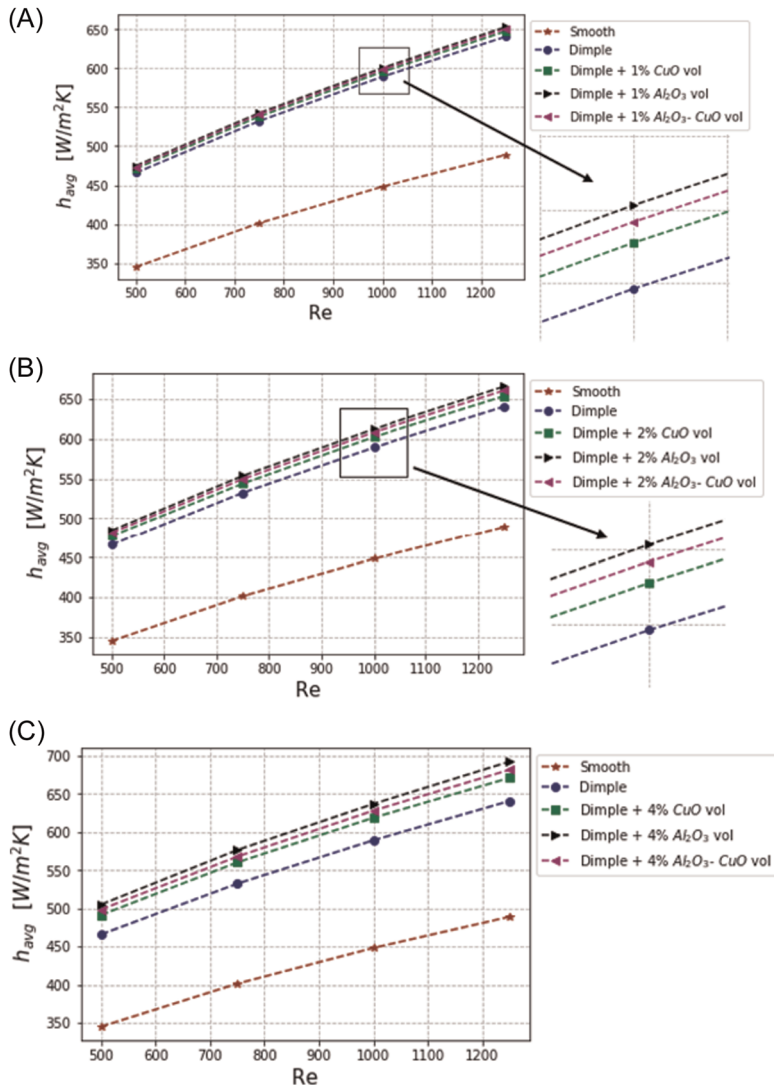

FIGURE 13 Variation of heat transfer coefficient with *Re* for nanofluids with (A) 1% vol, (B) 2% vol, and (C) 4% vol [Color figure can be viewed at wileyonlinelibrary.com]

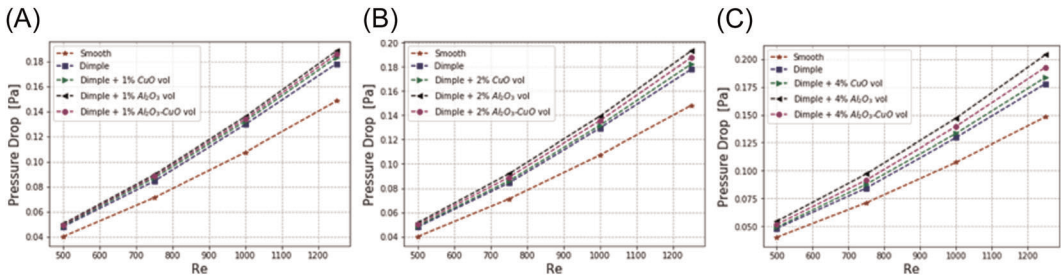

FIGURE 14 Pressure distribution along the centerline for (A) 1% vol, (B) 2% vol, and (C) 4% vol of each nanofluid with *Re* [Color figure can be viewed at wileyonlinelibrary.com]

nanofluid from Figure 14B,C. Due to the higher density and viscosity, the trends of getting higher pressure drop is observed with increasing volume fraction.

5.4 | Study of volumetric entropy generation

The calculation of volumetric entropy generation was extracted as

$$\Delta S \equiv \int_{\text{rev}} \frac{\delta Q}{T}, \tag{22}$$

where Q indicates the amount of heat and T represents temperature.

If the fluid is assumed to be compressible, then the entropy is calculated as

$$\Delta S = C_p \ln\left(\frac{T}{T_{\text{ref}}}\right) - R \ln\left(\frac{P}{P_{\text{ref}}}\right). \tag{23}$$

The equation could be simplified to the following equation[87] as

$$\Delta S = C_p \ln\left(\frac{T}{T_{\text{ref}}}\right), \tag{24}$$

where T_{ref} represents reference temperature and P_{ref} represents the reference pressure.

The variation of volumetric entropy generation for different coolants as a function of *Re* is represented in Figures 15 and 16. It is noted from the figures that volumetric entropy generation is higher in dimpled channels compared with smooth channels, and the value gradually decreases with an increase in Re. Besides, from Figure 15A–C, it is identified that for the dimpled channel, with the increase in volume fraction for each nanofluid, the volumetric entropy generation decreases and was found lowest for 4% vol of each nanofluid. The remarks could be drawn that an increase in volume fraction reduces the value of volumetric entropy generation for nanofluids. The observed variations in the above result due to the inclusion of nanoparticles could be explained by the improvement in thermophysical properties, such as high thermal conductivity.

Figure 16 represents the volumetric entropy generation with *Re* for different nanofluids at the same volume fraction. The objective of this investigation is to analyze the effect of thermophysical properties of individual nanofluids in entropy generation. From Figure 16A, the observation could be provided that Al_2O_3/water with 1% vol has the highest entropy generation, followed by Al_2O_3/water while 1% vol CuO/water has the lowest entropy generation. A similar phenomenon is observed for both the 2% and 4% volume fraction of each nanofluid in Figure 16B,C.

5.5 | Study of Nusselt number and friction factors

Figure 17 illustrates the variation of Nusselt number and friction factors through varying Re for each nanofluid. It is evident from Figure 17A that the value of Nu is predicted highest for 1% Al_2O_3/water, followed by Al_2O_3–CuO/water, and the lowest value is predicted for 1% CuO/water. Nevertheless, a similar trend is found for friction factors from Figure 17A, which exhibits

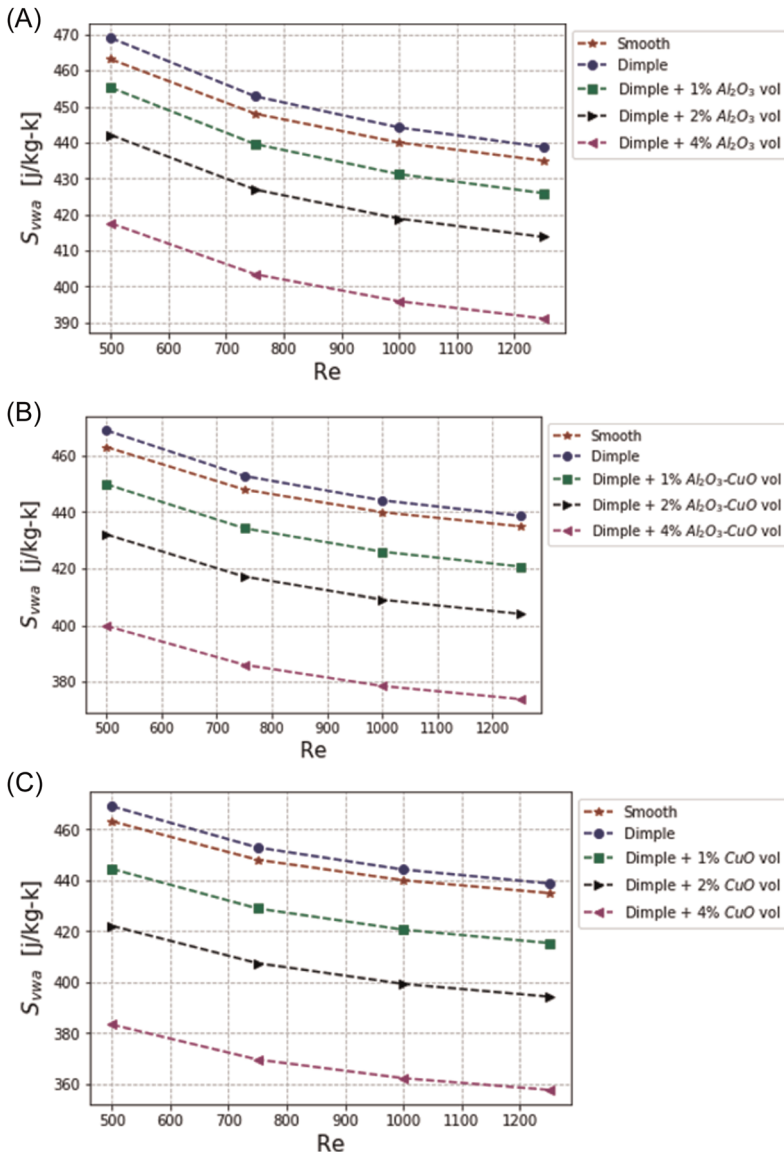

FIGURE 15 Variation of volumetric entropy generation for (A) Al_2O_3/water, (B) Al_2O_3–CuO/water, and (C) CuO/water [Color figure can be viewed at wileyonlinelibrary.com]

the highest friction factor for 1% Al_2O_3/water, superseded by Al_2O_3–CuO/water, and the lowest friction factor is observed for 1% CuO/water. As from the analysis of Figure 17B,C, an exhibition of a similar phenomenon is noticeable for both 2% and 4% of each nanofluid. As shown in Figure 13, the value of HTC is found highest for Al_2O_3/water, decreases for Al_2O_3-CuO/water, and lowest for CuO/water. Hence, the *Nu* numbers are increased with Re following similar trends as HTC, supported by the basic formulations used.[73,78–80] For the pressure drop also, a similar trend is noticed, as shown in Figure 14, which allows the friction factor to conform alike shift followed by relevant equation.[73,78–80]

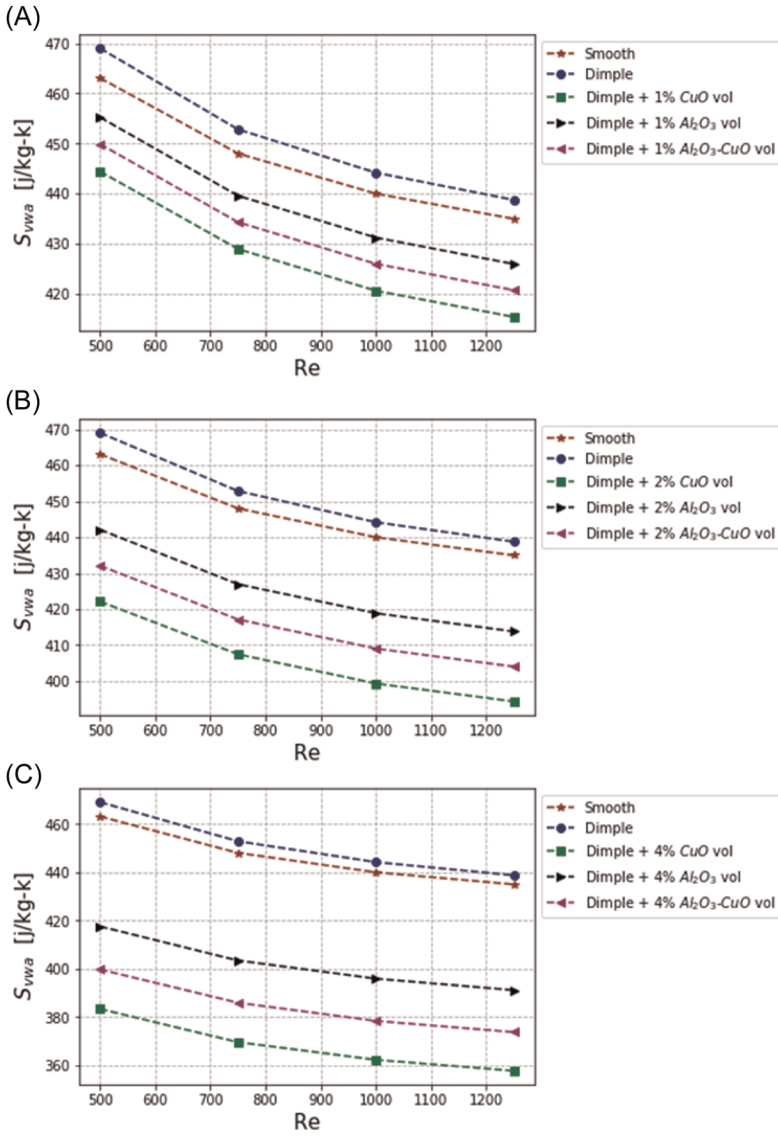

FIGURE 16 Variation of volumetric entropy generation for (A) 1% vol, (B) 2% vol, and (C) 4% vol of each nanofluid as a function of *Re* [Color figure can be viewed at wileyonlinelibrary.com]

5.6 | Study of PEC for nanofluids

The value of PEC accounts for both the pressure loss and enhancement in HTC to put a remark on the coolant.[73,78–80] From Figure 18A, it is noted that the value of PEC is found to be highest for 1% Al_2O_3/water, followed by 1% Al_2O_3–CuO/water, followed by 1% CuO/water. The value of PEC is found highest at $Re = 500$ and lowest at $Re = 1000$. Similar trends are observed for both 2% and 4% vol of each nanofluid from Figure 18B,C. An explanation could be made that due to a higher property enhancement ratio for Al_2O_3, the value of PEC is highest for Al_2O_3/water. On the contrary, the property enhancement ratio is lowest for CuO/water; hence the PEC is observed lowest. Nevertheless, the value of HTC is more dominant at $Re = 500$ and 1250

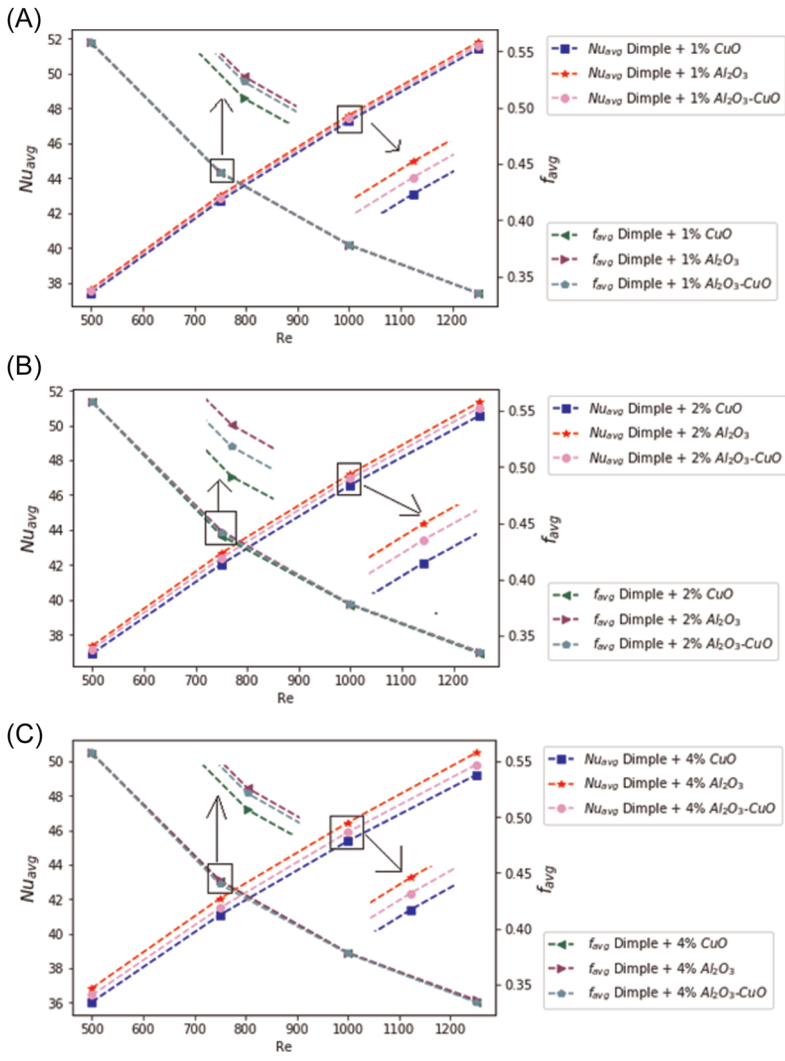

FIGURE 17 Variation of *Nu* number and friction factor with *Re* for (A) 1%, (B) 2%, and (C) 3% vol of each nanofluid [Color figure can be viewed at wileyonlinelibrary.com]

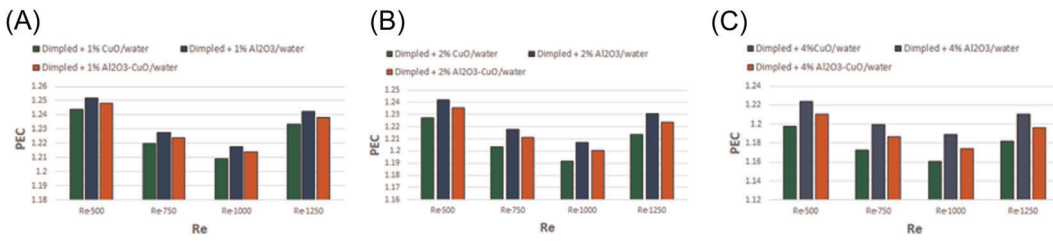

FIGURE 18 Variation of performance evaluation criteria with *Re* for (A) 1%, (B) 2%, and (C) 4% vol of each nanofluid [Color figure can be viewed at wileyonlinelibrary.com]

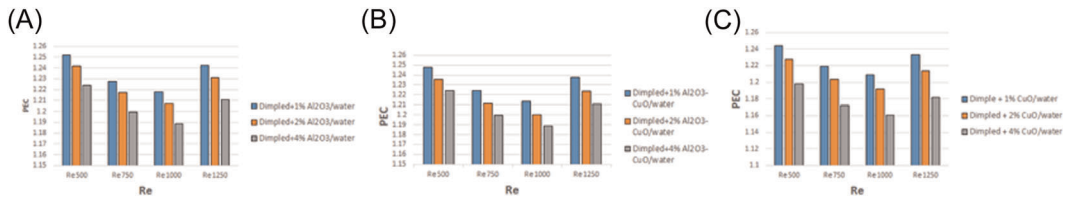

FIGURE 19 Variation of performance evaluation criteria for (A) Al_2O_3/water, (B) Al_2O_3–CuO/water, and (C) CuO/water [Color figure can be viewed at wileyonlinelibrary.com]

compared with the pressure loss created by density. On the other hand, at $Re = 750$ and 1000, the pressure drop is found dominant compared with heat transfer enhancement. Hence, the highest PEC is observed at $Re = 500$ and lowest at $Re = 750$. From this study, it can be concluded that to get the highest thermal performance in the dimpled channel test section; the suitable coolant is Al_2O_3 at low velocities.

From Figure 19, it is evident that an increase in each nanofluid's volume fraction leads to a decrease in PEC value.[88] This phenomenon will make density and pressure drop to be dominant. Hence, the value of PEC decreases with the increase in volume fraction for the present dimpled test section.[49] The conclusion could be drawn evaluating thermal performance that 1% volume fraction will lead to the highest efficiency at $Re = 500$.

6 | CONCLUSION

In this study, we investigated the performance of the dimpled channel for the enhancement of heat transfer performance in the presence of nanofluid coolants. The main conclusions of the study are-

- In contrast to the smooth channel, the HTC value is found 35.06% higher for the dimpled channel at $Re = 500$ for the base fluid. The value of HTC is found 37.70%, 40.53%, and 46.41% higher for 1%, 2%, and 4% Al_2O_3 nanofluid compared with the base fluid at $Re = 500$. Again the HTC value is seen as 37.24%, 39.67%, and 44.54% higher for 1%, 2%, and 4% Al_2O_3–CuO nanofluid successively. For CuO nanofluid, the value of HTC is increased to 36.63%, 38.5%, and 42.43% at $Re = 500$ for 1%, 2%, and 4%, consecutively.
- The increase in volume fraction for each nanofluid leads to the reduction in the volumetric entropy generation. Besides, the volumetric entropy generation at 1%, 2%, and 4% was observed highest for Al_2O_3/water, followed by Al_2O_3–CuO/water, and least for CuO/water.
- The PEC is observed as decreasing with the increase in volume fraction.
- Among the nanofluids, the highest PEC is observed as 25.18% higher compared with the base fluid for 1% Al_2O_3/water at $Re = 500$. The value of PEC is seen as 24.8% higher for 1% Al_2O_3–CuO/water and 24.40% higher for 1% CuO/water compared with the base fluid at $Re = 500$.

Hence, the study proposes that Al_2O_3/water with a 1% volume fraction at $Re = 500$ is the most efficient one for the heat transfer in the dimpled channel. It is also concluded that Al_2O_3–CuO/water (with an equal mixture ratio for Al_2O_3 and CuO particles) hybrid nanofluid are showing lower thermal performance when compared with Al_2O_3/water nanofluid.

NOMENCLATURE

CFD	computational fluid dynamics
e/d	ratio of dimple depth to dimpled diameter
HTC	heat transfer coefficient
PEC	performance evaluation criterion
PER	properties enhancement ratio
x/d	streamwise spacing
y/d	spanwise spacing
$\mathfrak{V}$	velocity (m/s)
c_p	specific heat of fluid (J/kg K)
D_h	hydraulic diameter
P	pressure (N/m^2)
q	wall heat flux (W/m^2)
T	temperature (K)
Nu	Nusselt number
Pr	Prandtl number
Re	Reynolds number
μ	dynamic viscosity ($(N{\cdot}s)/m^2$)
ν	kinematic viscosity (m^2/s)
ρ	density (kg/m^3)
φ	nanoparticle volume fraction
k	thermal conductivity ($W\ m^{-1}\ K^{-1}$)

Subscripts

i, j, k	tensor index
bf	base fuel
nf	nanofluid
hnf	hybrid nanofluid
b	bulk
w	wall
ref	reference value
Rev	integration along a reversible path connecting two states
np	nanoparticle
avg	averaged
vwa	volume weighted averaged
0	initial value
z	flow direction, velocity components u, v, and w in x, y, and z directions

REFERENCES

1. Karimipour A, Bagherzadeh SA, Taghipour A, Abdollahi A, Safaei MR. A novel nonlinear regression model of SVR as a substitute for ann to predict conductivity of MWCNT-CuO/water hybrid nanofluid based on empirical data. *Physica A Stat Mech Appl*. 2019;521:89-97.
2. Goodarzi H, Akbari OA, Sarafraz MM, Karchegani MM, Safaei MR, SheikhShabani GA. Numerical simulation of natural convection heat transfer of nanofluid with Cu, MWCNT, and Al_2O_3 nanoparticles in a cavity with different aspect ratios. *J Therm Sci Eng Appl*. 2019;11:6.

3. Akbari OA, Safaei MR, Goodarzi M, Akbar NS, Zarringhalam M, Shabani GAS, Dahari M. A modified two-phase mixture model of nanofluid flow and heat transfer in a 3-d curved microtube. *Adv Powder Technol*. 2016;27(5):2175-2185.
4. Karimipour A, Hossein AN, D'Orazio A, Esfe MH, Safaei MR, Shirani E. Simulation of copper-water nanofluid in a microchannel in slip flow regime using the lattice Boltzmann method. *Eur J Mech B Fluids*. 2015;49:89-99.
5. Akbari OA, Toghraie D, Karimipour A. Impact of ribs on flow parameters and laminar heat transfer of water-aluminum oxide nanofluid with different nanoparticle volume fractions in a three-dimensional rectangular microchannel. *Nat Energy*. 2015;7(11):1687814015618155.
6. Ahmed F, Abir MA, Redwan A, Bhuiyan AA, Mollah A. The impact of d-shaped jaggedness on heat transfer enhancement technique using al_2o_3 based nanoparticles. *Int J Thermofluids*. 2021;10:100069.
7. Hwang SD, Kwon HG, Cho HH. Local heat transfer and thermal performance on periodically dimple-protrusion patterned walls for compact heat exchangers. *Energy*. 2010;35(12):5357-5364.
8. Abdollahi A, Darvanjooghi MHK, Karimipour A, Safaei MR. Experimental study to obtain the viscosity of CuO-loaded nanofluid: effects of nanoparticles' mass fraction, temperature and basefluids types to develop a correlation. *Meccanica*. 2018;53(15):3739-3757.
9. Safaei M, Togun H, Vafai K, Kazi S, Badarudin A. Investigation of heat transfer enhancement in a forward-facing contracting channel using FMWCNT nanofluids. *Numer Heat Transfer A Appl*. 2014;66(12):1321-1340.
10. Laitinen A, Peltonen P, Vuorinen V. Computational fluid dynamics simulations of liquid cooling for electronics; 2018.
11. Tuckerman D, Pease R. High-performance heat sinking for VLSI. *IEEE Electron Device Lett*. 1981;2(5):126-129.
12. Lan J, Xie Y, Zhang D. Flow and heat transfer in microchannels with dimples and protrusions. *J Heat Transfer*. 2012;134(2):021901.
13. Aminossadati S, Raisi A, Ghasemi B. Effects of magnetic field on nanofluid forced convection in a partially heated microchannel. *Int J Non-Linear Mech*. 2011;46(10):1373-1382.
14. Huminic G, Huminic A. Hybrid nanofluids for heat transfer applications—a state-of-the-art review. *Int J Heat Mass Transfer*. 2018;125:82-103.
15. Han J-C, Dutta S, Ekkad S. *Gas Turbine Heat Transfer and Cooling Technology*. New York: Taylor & Francis; 2012.
16. Ligrani PM, Oliveira MM, Blaskovich T. Comparison of heat transfer augmentation techniques. *AIAA J*. 2003;41(3):337-362.
17. Chyu MK, Yu Y, Ding H, Downs JP, Soechting FO. Concavity enhanced heat transfer in an internal cooling passage. *Proceedings of the ASME 1997 International Gas Turbine and Aeroengine Congress and Exhibition. Vol. 3: Heat Transfer, Electric Power, Industrial and Cogeneration*. Orlando, Florida, USA; 1997. V003T09A080. ASME.
18. Li B-D, Liu P, Zheng N-B, Liu Z-C, Liu W. Numerical simulation of helically dimpled tubes for convection heat transfer and pressure drop. *J Eng Thermophys*. 2016;37(6):1261-1267.
19. Siddique M, Khaled A-R, Abdulhafiz N, Boukhary A. Recent advances in heat transfer enhancements: a review report. *Int J Chem Eng*. 2010;2010:1-28.
20. Ganjbakhsh N, Alikhani S, Behzadmehr A. Numerical study of the effects of surface roughness on the mixed convection heat transfer of a laminar flow inside a horizontal curved dimpled tube. *Heat Mass Transfer*. 2019;55(7):2009-2016.
21. Kasaeian A, Daviran S, Azarian RD, Rashidi A. Performance evaluation and nanofluid using capability study of a solar parabolic trough collector. *Energy Convers Manag*. 2015;89:368-375.
22. Motlagh SY, Golab E, Sadr AN. Two-phase modeling of the free convection of nanofluid inside the inclined porous semi-annulus enclosure. *Int J Mech Sci*. 2019;164:105183.
23. Aminian E, Moghadasi H, Saffari H. Magnetic field effects on forced convection flow of a hybrid nanofluid in a Q15 cylinder filled with porous media: a numerical study. *J Therm Anal Calorim*. 2020;141(5):1-13.
24. Ahmadi AA, Khodabandeh E, Moghadasi H, Malekian N, Akbari OA, Bahiraei M. Numerical study of flow and heat transfer of water-Al_2O_3 nanofluid inside a channel with an inner cylinder using Eulerian-Lagrangian approach. *J Therm Anal Calorim*. 2018;132(1):651-665.

25. Kaood A, Hassan MA. Thermo-hydraulic performance of nanofluids flow in various internally corrugated tubes. *Chem Eng Process Process Intens*. 2020;154:108043.
26. Malekian S, Fathi E, Malekian N, Moghadasi H, Moghimi M. Analytical and numerical investigations of unsteady graphene oxide nanofluid flow between two parallel plates. *Int J Thermophys*. 2018;39(9):100.
27. Siavashi M, Bahrami HRT, Aminian E. Optimization of heat transfer enhancement and pumping power of a heat exchanger tube using nanofluid with gradient and multi-layered porous foams. *Appl Therm Eng*. 2018;138:465-474.
28. Siavashi M, Bahrami HRT, Aminian E, Saffari H. Numerical analysis on forced convection enhancement in an annulus using porous ribs and nanoparticle addition to base fluid. *J Cent South Univ*. 2019;26(5):1089-1098.
29. Xuan Y, Li Q. Investigation on convective heat transfer and flow features of nanofluids. *J Heat Transfer*. 2003;125(1):151-155.
30. Moshizi S, Malvandi A, Ganji D, Pop I. A two-phase theoretical study of Al_2O_3-water nanofluid flow inside a concentric pipe with heat generation/absorption. *Int J Therm Sci*. 2014;84:347-357.
31. Goodarzi M, Safaei M, Vafai K, Ahmadi G, Dahari M, Kazi S, Jomhari N. Investigation of nanofluid mixed convection in a shallow cavity using a two-phase mixture model. *Int J Therm Sci*. 2014;75:204-220.
32. Safaei MR, Safdari Shadloo M, Goodarzi MS, Hadjadj A, Goshayeshi HR, Afrand M, Kazi S. A survey on experimental and numerical studies of convection heat transfer of nanofluids inside closed conduits. *Adv Mech Eng*. 2016;8(10):1687814016673569.
33. Peng Y, Khaled U, Al-Rashed AAAA, Meer R, Goodarzi M, Sarafraz MM. Potential application of Response Surface Methodology (RSM) for the prediction and optimization of thermal conductivity of aqueous CuO (II) nanofluid: a statistical approach and experimental validation. *Phys A Stat Mech Appl*. 2020;554. https://doi.org/10.1016/j.physa.2020.124353
34. Li Z, Sarafraz M, Mazinani A, Hayat T, Alsulami H, Goodarzi M. Pool boiling heat transfer to CuO-H_2O nanofluid on finned surfaces. *Int J Heat Mass Transfer*. 2020;156:119780.
35. Malvandi A, Safaei M, Kaffash M, Ganji D. Mhd mixed convection in a vertical annulus filled with Al_2O_3-water nanofluid considering nanoparticle migration. *J Magn Magn Mater*. 2015;382:296-306.
36. Peng Y, Parsian A, Khodadadi H, Akbari M, Ghani K, Goodarzi M, Bach Q-V. Develop optimal network topology of artificial neural network (AONN) to predict the hybrid nanofluids thermal conductivity according to the empirical data of Al_2O_3-Cu nanoparticles dispersed in ethylene glycol. *Phys A Stat Mech Appl*. 2020;549. https://doi.org/10.1016/j.physa.2019.124015
37. Devi SSU, Devi SA. Numerical investigation of three-dimensional hybrid Cu-Al_2O_3/water nanofluid flow over a stretching sheet with effecting Lorentz force subject to Newtonian heating. *Can J Phys*. 2016;94(5):490-496.
38. Izadi M, Mohebbi R, Delouei AA, Sajjadi H. Natural convection of a magnetizable hybrid nanofluid inside a porous enclosure subjected to two variable magnetic fields. *Int J Mech Sci*. 2019;151:154-169.
39. Gheynani AR, Akbari OA, Zarringhalam M, Shabani GAS, Alnaqi AA, Goodarzi M, Toghraie D. Investigating the effect of nanoparticles diameter on turbulent flow and heat transfer properties of non-newtonian carboxymethyl cellulose/CuO fluid in a microtube. *Int J Numer Method Heat Fluid Flow*. 2019;29(5):1699-1723.
40. Aladdin NAL, Bachok N, Pop I. Cu-Al_2O_3/water hybrid nanofluid flow over a permeable moving surface in presence of hydromagnetic and suction effects. *Alex Eng J*. 2020;59(2):657-666.
41. Suresh S, Venkitaraj K, Selvakumar P, Chandrasekar M. Synthesis of Al_2O_3-Cu/water hybrid nanofluids using two step method and its thermo physical properties. *Colloids Surf A Physicochem Eng Aspects*. 2011;388(1-3):41-48.
42. Esfe MH, Alirezaie A, Rejvani M. An applicable study on the thermal conductivity of SWCNT-MgO hybrid nanofluid and price-performance analysis for energy management. *Appl Therm Eng*. 2017;111:1202-1210.
43. Madhesh D, Parameshwaran R, Kalaiselvam S. Experimental investigation on convective heat transfer and rheological characteristics of Cu-TiO_2 hybrid nanofluids. *Exp Therm Fluid Sci*. 2014;52:104-115.
44. Nine MJ, Batmunkh M, Kim J-H, Chung H-S, Jeong H-M. Investigation of Al_2O_3-MWCNTs hybrid dispersion in water and their thermal characterization. *J Nanosci Nanotechnol*. 2012;12(6):4553-4559.
45. Siddiqui FR, Tso CY, Fu SC, Qiu H, Chao CY. Evaporation and wetting behavior of silver-graphene hybrid nanofluid droplet on its porous residue surface for various mixing ratios. *Int J Heat Mass Transfer*. 2020;153:119618.

46. Moghadassi A, Ghomi E, Parvizian F. A numerical study of water based Al_2O_3 and Al_2O_3-Cu hybrid nanofluid effect on forced convective heat transfer. *Int J Therm Sci*. 2015;92:50-57.
47. Bahiraei M, Mazaheri N, Hanooni M. Performance enhancement of a triple-tube heat exchanger through heat transfer intensification using novel crimped-spiral ribs and nanofluid: a two-phase analysis. *Chem Eng Process Process Intens*. 2021;160:108289.
48. Anuar NS, Bachok N, Pop I. Cu-Al_2O_3/water hybrid nanofluid stagnation point flow past MHD stretching/shrinking sheet in presence of homogeneous-heterogeneous and convective boundary conditions. *Mathematics*. 2020;8(8):1237.
49. Etaig S. *Investigation of the Enhancement of Convective Heat Transfer for Wall-Bounded Flows Utilizing Nanofluids* [Ph.D. dissertation]. Newcastle upon Tyne: Northumbria University; 2017.
50. Sarkar J. A critical review on convective heat transfer correlations of nanofluids. *Renew Sustain Energy Rev*. 2011;15(6):3271-3277.
51. Massoudi M, Phuoc TX. Remarks on constitutive modeling of nanofluids. *Adv Mech Eng*. 2012;4:927580.
52. Eastman JA, Phillpot S, Choi S, Keblinski P. Thermal transport in nanofluids. *Annu Rev Mater Res*. 2004;34:219-246.
53. Behroyan I, Ganesan P, He S, Sivasankaran S. Turbulent forced convection of Cu-water nanofluid: CFD model comparison. *Int Commun Heat Mass Transfer*. 2015;67:163-172.
54. Bianco V, Manca O, Nardini S. Numerical investigation on nanofluids turbulent convection heat transfer inside a circular tube. *Int J Therm Sci*. 2011;50(3):341-349.
55. Nazififard M, Nematollahi M, Suh KY. Numerical analysis of water-based nanofluid coolant for small modular reactor. *Proceedings of the ASME 2011 Small Modular Reactors Symposium*. Washington, DC, USA; 2011:199-205. ASME.
56. Bianco V, Chiacchio F, Manca O, Nardini S. Numerical investigation of nanofluids forced convection in circular tubes. *Appl Therm Eng*. 2009;29(17-18):3632-3642.
57. Bianco V, Nardini S, Manca O. Enhancement of heat transfer and entropy generation analysis of nanofluids turbulent convection flow in square section tubes. *Nanoscale Res Lett*. 2011;6(1):252.
58. Bianco V, Manca O, Nardini S. Numerical simulation of water/Al_2O_3 nanofluid turbulent convection. *Adv Mech Eng*. 2010;2:976254.
59. Shabgard H, Kheradmand S, Farzaneh H, Bae C. Numerical simulation of cooling performance of an exhaust gas recirculation (EGR) cooler using nano-fluids. *Appl Therm Eng*. 2017;110:244-252.
60. Behzadmehr A, Saffar-Avval M, Galanis N. Prediction of turbulent forced convection of a nanofluid in a tube with uniform heat flux using a two phase approach. *Int J Heat Fluid Flow*. 2007;28(2):211-219.
61. Corcione M, Cianfrini M, Quintino A. Heat transfer of nanofluids in turbulent pipe flow. *Int J Therm Sci*. 2012;56:58-69.
62. Maïga SEB, Nguyen CT, Galanis N, Roy G, Maré T, Coqueux M. Heat transfer enhancement in turbulent tube flow using Al_2O_3 nanoparticle suspension. *Int J Numer Method Heat Fluid Flow*. 2006;16(3):275-292.
63. Bibi A, Xu H, Sun Q, Pop I, Zhao Q. Free convection of a hybrid nanofluid past a vertical plate embedded in a porous medium with anisotropic permeability. *Int J Numer Method Heat Fluid Flow*. 2019;30(8):4083-4101.
64. Nazififard M, Nematollahi M, Jafarpour K, Suh KY. Augmented safety heat transport in research reactor ir-40 using nanofluid. *Atw Internationale Zeitschrift fuer Kernenergie*. 2012;58(4):262-270.
65. Pak BC, Cho YI. Hydrodynamic and heat transfer study of dispersed fluids with submicron metallic oxide particles. *Exp Heat Transfer Int J*. 1998;11(2):151-170.
66. Brinkman H. The viscosity of concentrated suspensions and solutions. *J Chem Phys*. 1952;20(4):571.
67. Hamilton RL, Crosser O. Thermal conductivity of heterogeneous two-component systems. *Ind Eng Chem Fund*. 1962;1(3):187-191.
68. Yu W, Choi S. The role of interfacial layers in the enhanced thermal conductivity of nanofluids: a renovated Maxwell model. *J Nanoparticle Res*. 2003;5(1-2):167-171.
69. Moghadasi H, Aminian E, Saffari H, Mahjoorghani M, Emamifar A. Numerical analysis on laminar forced convection improvement of hybrid nanofluid within a U-bend pipe in porous media. *Int J Mech Sci*. 2020:105659.
70. Sarlak R, Yousefzadeh S, Akbari OA, Toghraie D, Sarlak S, et al. The investigation of simultaneous heat transfer of water/Al_2O_3 nanofluid in a close enclosure by applying homogeneous magnetic field. *Int J Mech Sci*. 2017;133:674-688.

71. Alipour Lalami A, Hassanzadeh Afrouzi H, Moshfegh A, Omidi M, Javadzadegan A. Investigation of nanofluid heat transfer in a microchannel under magnetic field via lattice Boltzmann method: effects of surface hydrophobicity, viscous dissipation, and joule heating. *J Heat Transfer*. 2019;141(6). https://doi.org/10.1115/1.4043163
72. Dinarvand S, Rostami MN, Pop I. A novel hybridity model for TiO_2-CuO/water hybrid nanofluid flow over a static/moving wedge or corner. *Sci Rep*. 2019;9(1):1-11.
73. Vajjha RS, Das DK, Kulkarni DP. Development of new correlations for convective heat transfer and friction factor in turbulent regime for nanofluids. *Int J Heat Mass Transfer*. 2010;53(21-22):4607-4618.
74. Yazdanifard F, Ameri M, Ebrahimnia-Bajestan E. Performance of nanofluid-based photovoltaic/thermal systems: a review. *Renew Sustain Energy Rev*. 2017;76:323-352.
75. Akbari OA, Toghraie D, Karimipour A, Safaei MR, Goodarzi M, Alipour H, Dahari M. Investigation of rib's height effect on heat transfer and flow parameters of laminar water-Al_2O_3 nanofluid in a rib-microchannel. *Appl Math Comput*. 2016;290:135-153.
76. Kumar S, Kothiyal AD, Bisht MS, Kumar A. Turbulent heat transfer and nanofluid flow in a protruded ribbed square passage. *Results Phys*. 2017;7:3603-3618.
77. Kandlikar SG. Microchannels and minichannels-history, terminology, classification and current research needs. *In First International Conference on Microchannels and Minichannels*. New York; 2003.
78. Majid S, Mohammad J. Optimal selection of annulus radius ratio to enhance heat transfer with minimum entropy generation in developing laminar forced convection of water-Al_2O_3 nanofluid flow. *J Cent South Univ*. 2017;24(8):1850-1865.
79. Ganji DD, Malvandi A. *Heat Transfer Enhancement Using Nanofluid Flow in Microchannels: Simulation of Heat and Mass Transfer*. Norwich, NY: William Andrew; 2016.
80. Minkowycz W, Sparrow E. *Series in Computational and Physical Processes in Mechanics and Thermal Sciences*. New York: Taylor & Francis; 1993.
81. Stephan K, Preußer P. Wärmeübergang und maximale wärmestromdichte beim behältersieden binärer und ternärer flüssigkeitsgemische; 1979.
82. Barnoon P, Toghraie D. Numerical investigation of laminar flow and heat transfer of non-newtonian nanofluid within a porous medium. *Powder Technol*. 2018;325:78-91.
83. Azari A, Kalbasi M, Derakhshandeh M, Rahimi M. An experimental study on nanofluids convective heat transfer through a straight tube under constant heat flux. *Chin J Chem Eng*. 2013;21(10):1082-1088.
84. Shah R. Thermal entry length solutions for the circular tube and parallel plates. In: *Proceedings of 3rd national heat and mass transfer conference*, Vol. 1. Indian Institute of Technology Bombay; 1975:HMT-11.
85. Safaei MR, Gooarzi M, Akbari OA, Shadloo MS, Dahari M. Performance evaluation of nanofluids in an inclined ribbed microchannel for electronic cooling applications. In: Sohel Murshed SM, ed. *Electronics Cooling*. IntechOpen; 2016. https://doi.org/10.5772/62898. Available from: https://www.intechopen.com/books/electronics-cooling/performance-evaluation-of-nanofluids-in-an-inclined-ribbed-microchannel-for-electronic-cooling-appli
86. Meyer JP, Adio SA, Sharifpur M, Nwosu PN. The viscosity of nanofluids: a review of the theoretical, empirical, and numerical models. *Heat Transfer Eng*. 2016;37(5):387-421.
87. ANSYS. *ANSYS Fluent User's. Guide*. Release 14.0, Canonsburg, PA: ANSYS. 2011.
88. Alashkar A. *Evaluation of an Integrated PTSC/Thermal Energy Storage System Using Nano-Fluid Particles* [Ph.D. dissertation]. Sharjah, United Arab Emirates: American University of Sharjah; 2016.

How to cite this article: Ahmed F, Abir MA, Fuad M, et al. Numerical investigation of the thermo-hydraulic performance of water-based nanofluids in a dimpled channel flow using Al_2O_3, CuO, and hybrid Al_2O_3–CuO as nanoparticles. *Heat Transfer*. 2021;50:5080-5105. https://doi.org/10.1002/htj.22116